Regularities of behavior of temperature dependences of resistivity of crystals of solid solutions $(Bi_{2-x}Sb_x)Te_3$ $(0 < x < 2)$

© N.P. Stepanov[1], M.S. Ivanov[2], L.E. Stepanova[1], L.V. Vinogradova[2]

[1] Trans-Baikal State University,
672036 Chita, Russia
[2] Trans-Baikal Institute of Railway Transport,
672040 Chita, Russia

E-mail: np-stepanov@mail.ru

Received March 22, 2022
Revised June 21, 2022
Accepted July 8, 2022

It is shown that the change in the resistivity of crystals of solid solutions $(Bi_{2-x}Sb_x)Te_3$ $(0 < x < 2)$ *p*-type in the temperature range preceding the onset of intrinsic conductivity is due not only to a change in the static relaxation time, the behavior of which in the temperature range from 80 to 300 K is determined mainly by carrier scattering on the vibrations of the crystal lattice, but also by changing the concentration of light holes. The latter is a consequence of the transition of charge carriers from the subzone of heavy holes to the subzone of light holes, as a result of which the concentration of light holes, which make the main contribution to electrical conductivity, decreases with increasing temperature. As a consequence, the plasmon energy proportional to the concentration of charge carriers also decreases with increasing temperature, and the energy of this transition, comparable to the plasmon energy, increases. In this regard, crystals $(Bi_{2-x}Sb_x)Te_3$ have a specific feature due to the convergence of the plasmon energy and the interband transition, which creates conditions for increasing the intensity of the electron-plasmon interaction.

Keywords: thermoelectric materials, bismuth and antimony tellurides, resistivity, interband transitions, plasma of free charge carriers.

DOI: 10.21883/SC.2022.09.54214.9839

1. Introduction

Extensive studies of crystals of $(Bi_{2-x}Sb_x)Te_3$ $(0 < x < 2)$ solid solutions, which are used in commercial manufacture of thermoelectric energy converters, provided a wealth of data on their physical properties [1–8]. It is known that both *n*-type and *p*-type $(Bi_{2-x}Sb_x)Te_3$ crystals may be produced by adjusting the stoichiometry [1]. Special attention is paid to the examination of physical properties of *p*-type crystals, since they provide relatively high values of thermoelectric efficiency coefficient $Z = \alpha^2\sigma/\kappa$, which depends on thermal emf α, electric conductivity σ, and thermal conductivity κ. For example, it was reported in [2] that the Z value of a *p*-type $(Bi_{2-x}Sb_x)Te_3$ crystal with $x = 1.5$ is as high as $3.2 \cdot 10^{-3}\,K^{-1}$. The observed values of α, σ, and κ are largely defined by the band structure of these materials, which is presented in Fig. 1 and is characterized by the presence of nonequivalent carrier extrema in the valence band [7]. The numerical values of energy gaps indicated in Fig. 1 were taken from [9].

The complex structure of the valence band also affects the temperature dependences of physical quantities governing the thermoelectric efficiency of $(Bi_{2-x}Sb_x)Te_3$ crystals. In view of this, temperature dependences of the thermal emf, the thermal conductivity, and the electric conductivity may be used to examine the processes occurring in their electron system amid variations of temperature and the solid solution composition. Such studies are, first and foremost, of practical interest, since the issue of fabrication of more efficient thermoelectric materials remains topical. It is the current understanding that an empirical search for new thermoelectric materials cannot result in any significant enhancement of the thermoelectric efficiency; $(Bi_{2-x}Sb_x)Te_3$ crystals remain unrivaled in terms of a combination of parameters affecting the value of Z and are thus used widely in thermoelectric industry. In view of this, it appears practical to examine the processes in their electron system, which occur amid variations of temperature and the solid solution composition, with the aim of identifying the specific features of this material.

It is also reasonable to analyze the variation of electric conductivity first. This is attributable in part to the fact that the other physical quantities characterizing the state of the electron system are harder to interpret. For example, one needs to take a large number of temperature-dependent parameters into account in order to analyze the temperature dependence of the thermoelectric coefficient, which has bulk and contact components. In analyzing the thermal conductivity coefficient, which is shaped by contributions of the ion core and free carriers, bipolar diffusion, and the specifics of transport phenomena in semiconductors with a complex structure of the valence band, one is again required to consider a large number of influencing factors and heat transport mechanisms. That said, there also exist a number of obstacles to interpretation of the temperature dependence of electric conductivity. However,

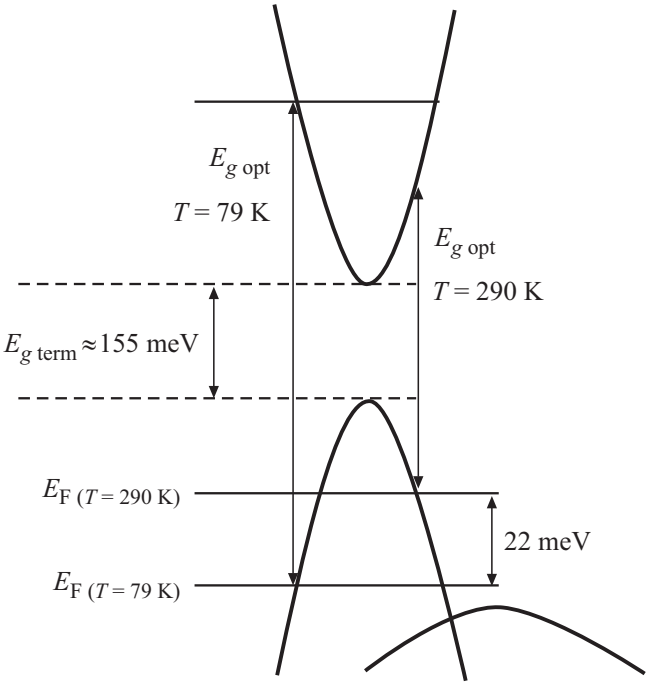

Figure 1. Band structure of $Bi_{0.8}Sb_{1.2}Te_3$ crystals and optical band gap values at different temperatures determined based on the results of optical studies in the infrared range [9].

since it is defined by variations of the concentration of free carriers, the results of experimental Hall measurements, the procedure and technique of which have been perfected over the years, may provide additional relevant information (including carrier mobility data). At the same time, the mobility value is affected by both the relaxation time and the effective mass, which is determined with a large error in most cases; this has a marked negative effect on the reliability of data on the steady-state relaxation time derived from mobility. In certain cases, however, data on the patterns of variation of the relaxation time help analyze the behavior of the electron system in finer detail. Theoretical calculations of the steady-state relaxation time in the considered materials are essentially infeasible, since $(Bi_{2-x}Sb_x)Te_3$ crystals (as well as bismuth and antimony crystals and bismuth–antimony alloys) were found to feature multivalley bands with different values of the effective mass and the density-of-state mass [10]. Therefore, intravalley, intervalley, interband, and recombination scattering may be significant. All of them combined may exert a certain influence on the steady-state relaxation time, and the ratio of their contributions depends on temperature. In view of this, experimental determination of steady-state relaxation time τ_{st} in $(Bi_{2-x}Sb_x)Te_3$ crystals is a relevant objective. It is known that this objective may be achieved by combining the results of experimental determination of electric conductivity σ and plasma frequency ω_p of free carriers. Since σ and ω_p depend on quantity $\sum_i (\frac{p_j}{m_j^*})$, which characterizes the sum of ratios of the free carrier concentration to their effective mass over all carrier groups, averaged steady-state relaxation time $\langle\tau_{st}\rangle$ may be determined as

$$\sigma = \sum_j \sigma_j = \sum_j \left(\frac{e^2 p \tau_{st}}{m^*}\right)_j$$

$$= \varepsilon_0 \varepsilon_\infty \sum_j (\omega_p^2 \tau_{st})_j = \varepsilon_0 \varepsilon_\infty \omega_p^2 \langle\tau_{st}\rangle, \qquad (1)$$

where e is the electron charge, ω_p is the plasma frequency, ε_∞ is the high-frequency permittivity, and ε_0 is the dielectric constant.

In view of this, the examination of characteristics of the plasma resonance of free carriers and the acquisition of experimental data on the value of $\sum_j (\frac{p_j}{m_j^*})$ may be the steps toward understanding the processes in the electron system of crystals of $(Bi_{2-x}Sb_x)Te_3$ $(0 < x < 2)$ solid solutions, which the aim of the present study.

2. Studied crystals; experimental procedure and technique

Single crystals of $Bi_{2-x}Sb_xTe_3$ $(0 < x < 2)$ solid solutions containing 25 and 60 mol% of Sb_2Te_3 and grown by the Czochralski method at the Baikov Institute of Metallurgy and Materials Science were studied [2]. In the present study, we report the results of examination of the optical properties of those crystals that had their temperature dependences of resistivity determined in [2]. A Bruker 113 V infrared Fourier spectrometer was used to obtain spectral dependences of the refection coefficient at radiation incidence angles no higher than 7° within the frequency range of 400–2500 cm^{-1} at fixed temperatures. The procedure and technique of the optical experiment were detailed in [11]. The real and imaginary parts of the permittivity function, which allow one to determine the plasma frequency, the high-frequency permittivity, and the optical relaxation time, were calculated based on the reflection spectra using the Kramers–Kronig relations. The electric conductivity of the studied samples was determined by the two-point probe method (at the same temperatures that were used to measure the reflection spectra) with all principal conditions of minimization of systematic and random measurement errors satisfied. The sample temperature was maintained to within 0.5 K.

3. Characterization and analysis of experimental results

Figure 2 shows the reflection spectra of the $Bi_{0.8}Sb_{1.2}Te_3$ crystal obtained at different temperatures in the $\mathbf{E} \perp C_3$ geometry, where C_3 is the trigonal crystal axis and $\mathbf{E}$ is the electric-field vector of an electromagnetic wave. The reflected signal in this geometry of an optical experiment

Experimental values of $\omega_{p\perp}$, $\varepsilon_{\infty\perp}$, $\sigma_\perp$ and results of calculation of $\sum_j \left(\frac{p_j}{m_j^*}\right)$, τ_{st} for the $Bi_{1.5}Sb_{0.5}Te_3$ crystal. The values of $\sigma_\perp$ corresponds to the data obtained in [2]

T, K	$\omega_{p\perp} \cdot 10^{13}$, rad/s	$\varepsilon_{\infty\perp}$	$\frac{p}{m^*} \cdot 10^{56}$, $(m^3 \cdot kg)^{-1}$	$\sigma \cdot 10^{-6}$, $\Omega^{-1} \cdot m^{-1}$	$\overline{\tau}_{st} \cdot 10^{-13}$, s
85	8.20	54	1.25	0.517	3.280
150	7.52	60	1.17	0.323	2.183
200	6.91	62	1.02	0.211	1.622
300	6.21	64	0.85	0.070	0.649

is shaped by oscillations of free carriers about the ion core in the direction perpendicular to C_3 (i.e., the direction along which the measurements of electric conductivity $\sigma \perp$ were performed). The obtained values of $\sigma \perp$ for the $Bi_{1.5}Sb_{0.5}Te_3$ sample are listed in the table.

The infrared reflection spectra in Fig. 2 feature a well-marked plasma edge and a minimum that shifts toward lower frequencies with increasing temperature. The spectral position of the plasma minimum generally agrees with the data presented in [12,13]. Plasma frequency ω_p and high-frequency permittivity ε_∞, which characterizes the polarization background of a crystal in the high-frequency (relative to the plasma edge) spectral range, were derived from reflection spectra. The procedure for calculation of ω_p and ε_∞ based on reflection spectra was detailed in [10], and the values obtained for the $Bi_{1.5}Sb_{0.5}Te_3$ crystal are listed in the table. It is evident that ratio $\sum_j \left(\frac{p_j}{m_j^*}\right)$, which is calculated in accordance with the following expression:

$$(\omega_p)^2 = \frac{e^2}{\varepsilon_\infty \varepsilon_0} \sum_j \left(\frac{p_j}{m_j^*}\right), \qquad (2)$$

decreases with increasing temperature. The averaged steady-state relaxation time for the $Bi_{1.5}Sb_{0.5}Te_3$ crystal was calculated in accordance with (1) on the assumption that free carrier plasma also specifies the response of this crystal to a steady electric field. The calculation results are presented in the table and in Fig. 3, where model curves characterizing the temperature behavior of $\langle \tau_{st} \rangle$ of carriers in degenerate and nondegenerate states of the electron system are also shown.

Let us estimate the correspondence between the experimental temperature dependence and theoretical expectations. It is known from [1,14,15] that lattice scattering dominates over the impurity one at temperatures > 100 K in $(Bi_{2-x}Sb_x)Te_3$ $(0 < x < 2)$ crystals containing no dopants. According to the theoretical description of the acoustic scattering mechanism, the relaxation time is approximately proportional to T^{-1} for strongly degenerate carriers, while the dependence for nondegenerate carriers may be close to T^{-2}.

It can be seen from Fig. 3 that a T^{-1} dependence provides a much closer fit to the slope of the experimental

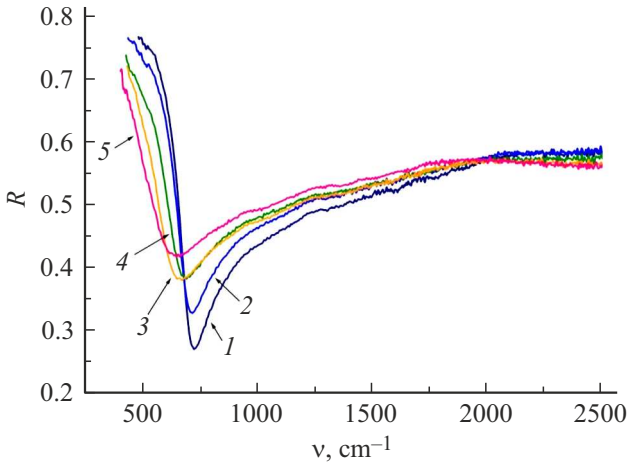

Figure 2. Spectral dependences of the reflection coefficient of the $Bi_{0.8}Sb_{1.2}Te_3$ crystal at various temperatures, K: *1* — 79, *2* — 93, *3* — 148, *4* – 213, *5* — 290.

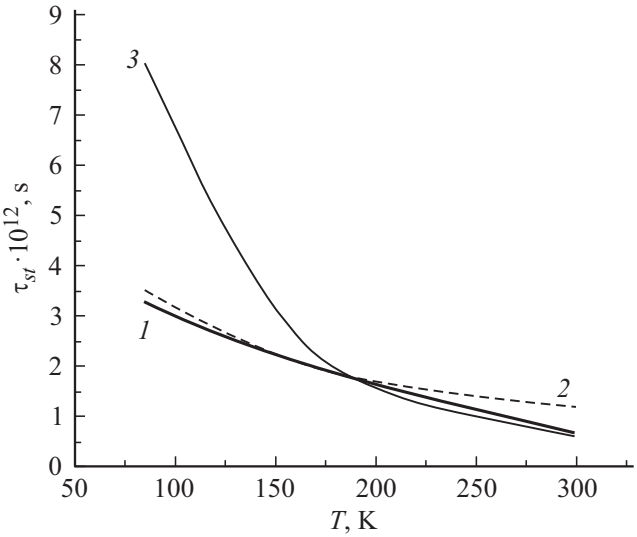

Figure 3. Temperature dependence of steady-state relaxation time τ_{st} of the $Bi_{1.5}Sb_{0.5}Te_3$ crystal (*1*) and model curves characterizing the behavior of $\tau_{st}(T)$ in degenerate (*2*) and nondegenerate (*3*) states of the electron system.

$\tau_{st}(T)$ curve in the temperature range from 85 to 150 K, while the slope of the curve at 200–300 K corresponds to T^{-2}. This agrees with the concept that carrier scattering off acoustic lattice vibrations is dominant in the studied crystal, degeneracy is lifted at a temperature of ~ 150 K, and intrinsic conductivity sets in at > 250 K [1]. Thus, there are reasons to believe that the obtained relaxation times of free carriers of the studied crystal in the temperature range from 85 to 300 K are defined primarily by their scattering off acoustic phonons; therefore, the contribution of other possible scattering mechanisms is negligible. It is fair to assume that such behavior of the steady-state relaxation time is typical of all $(Bi_{2-x}Sb_x)Te_3$ $(0 < x < 2)$ crystals grown

from high-purity components in accordance with one and the same technique.

If the pattern of variation of the steady-state relaxation time of free carriers in the vicinity of the Debye temperature is known, one may analyze the behavior of the electron system of $(Bi_{2-x}Sb_x)Te_3$ $(0 < x < 2)$ crystals using the data on the temperature dependence of their resistivity. These dependences are presented in Fig. 4 alongside with the data for metals, which agree well with the values calculated in accordance with the Bloch–Grüneisen expression [16]. The mentioned expression characterizes theoretically the temperature dependence of the part of electric resistivity attributable to the scattering of free carriers off thermal vibrations of the ion core:

$$\rho(T) = A\left(\frac{T}{\theta}\right)^5 \int_0^{\theta/T} \frac{z^5}{(e^z - 1)(1 - e^{-z})}\, dz, \qquad (3)$$

where $z = \hbar\omega/kT$, T is absolute temperature, A is a constant that characterizes the conductor type, and θ is the Debye temperature.

It was established experimentally that the Bloch–Grüneisen expression formulated without regard to anisotropy and other scattering mechanisms (e.g., scattering off impurities and other electrons) provides a fairly accurate description of the temperature variation of resistivity of pure metals [17].

Regardless of the fact that the average relaxation time in the considered temperature interval is, as follows from Fig. 3, governed by the carrier scattering off lattice vibrations, the dependences of resistivity of a series of $(Bi_{2-x}Sb_x)Te_3$ crystals in Fig. 4 deviate radically from the Bloch–Grüneisen model. Specifically, the resistivities of $(Bi_{2-x}Sb_x)Te_3$ crystals containing 0–50% of antimony telluride Sb_2Te_3 decrease with increasing temperature within certain high-temperature sections of the corresponding dependences; this is indicative of the onset of intrinsic conductivity. The transition to intrinsic conductivity in crystals containing $> 50\%$ Sb_2Te_3 is initiated at higher temperatures. This is attributable to the band gap widening and a shift of the chemical potential level deeper into the valence band, which leads to an increase in the carrier activation energy. A ~ 10-fold enhancement of the concentration of light holes in Sb_2Te_3 relative to the one in Bi_2Te_3 is also indicative of a shift of the chemical potential level deeper into the valence band, which is accompanied by a resistivity reduction (see the temperature dependences in Fig. 4).

Thus, when the percentage of antimony telluride increases, the temperature of transition to intrinsic conductivity also rises, thus expanding the temperature range within which the considered materials retain a high thermoelectric efficiency. The processes occurring in their electron system at temperatures up to the onset of intrinsic conductivity are of interest in this context. It can be seen from Fig. 4 that the rate of resistivity growth of $(Bi_{2-x}Sb_x)Te_3$ crystals in this temperature region is significantly higher than the one set by expression (3). An anomalous temperature dependence of the Hall coefficient [1], which is attributed most consistently to the transition of holes between nonequivalent extrema of the valence band, is also noted in the mentioned temperature region. This agrees with the observed reduction of $\sum_j \left(\frac{p_j}{m_j^*}\right)$ (see the data on its temperature variation in the table). As was demonstrated in [6], the reduction of $\sum_j \left(\frac{p_j}{m_j^*}\right)$ with increasing temperature cannot be attributed solely to an increase in the effective mass: it is necessary to introduce a reduction in the concentration of light holes at higher temperatures into the model. This is conceivable if the intensity of transition of electrons from the subband of heavy holes to the subband of light holes increases with temperature (the concentration of light holes decreases as a result, while the concentration of heavy ones increases). Experimental data in Fig. 2, where the energy of a diffuse high-frequency maximum of the reflection coefficient is seen to decrease with increasing temperature, verify the occurrence of such a transition of holes under temperature variation. Note that a reflection maximum observed in the high-frequency (relative to the plasma edge) spectral range is indicative of an enhanced crystal polarization, which is attributable to electron transitions from the valence band to the conduction band that shape the fundamental absorption edge. The transition energy reduction with increasing temperature may be attributed to a shift of the chemical potential level to the upper edge of the valence band due to the transition of electrons from the subband of heavy holes to the subband of light ones. With a simple structure of the valence and conduction bands, a temperature rise should result in an increase in the interband transition energy due to the Moss–Burstein effect. Therefore, the reduction in the interband transition energy at higher temperatures observed in Fig. 2 provides experimental evidence of the process of carrier transition between nonequivalent extrema of the valence band, which is accompanied by a reduction in the concentration of light holes with increasing temperature. This is also verified experimentally by the shift of the plasma minimum toward lower frequencies at higher temperatures (see Fig. 2), which suggests that the plasma frequency and, consequently, the concentration of light holes decrease.

Thus, the process of transition of holes between nonequivalent extrema of the valence band also affects the temperature dependence of resistivity of the studied materials, since it alters the $\sum_j \left(\frac{p_l}{m_j^*}\right)$ ratio. It is natural to assume that this influence is minimized at low temperatures close to 80 K: the energy of thermal vibrations $(kT \approx 7\,\text{meV})$ is still low here, and the variation of resistivity with temperature is governed by the temperature dependence of the relaxation time. Indeed, since energy gap ΔE between the chemical potential level and the upper edge of the subband of heavy holes in bismuth telluride crystals is $\sim 25-30\,\text{meV}$ [1], the energy of thermal vibrations at 80 K is ~ 4 times lower, and the transition probability is

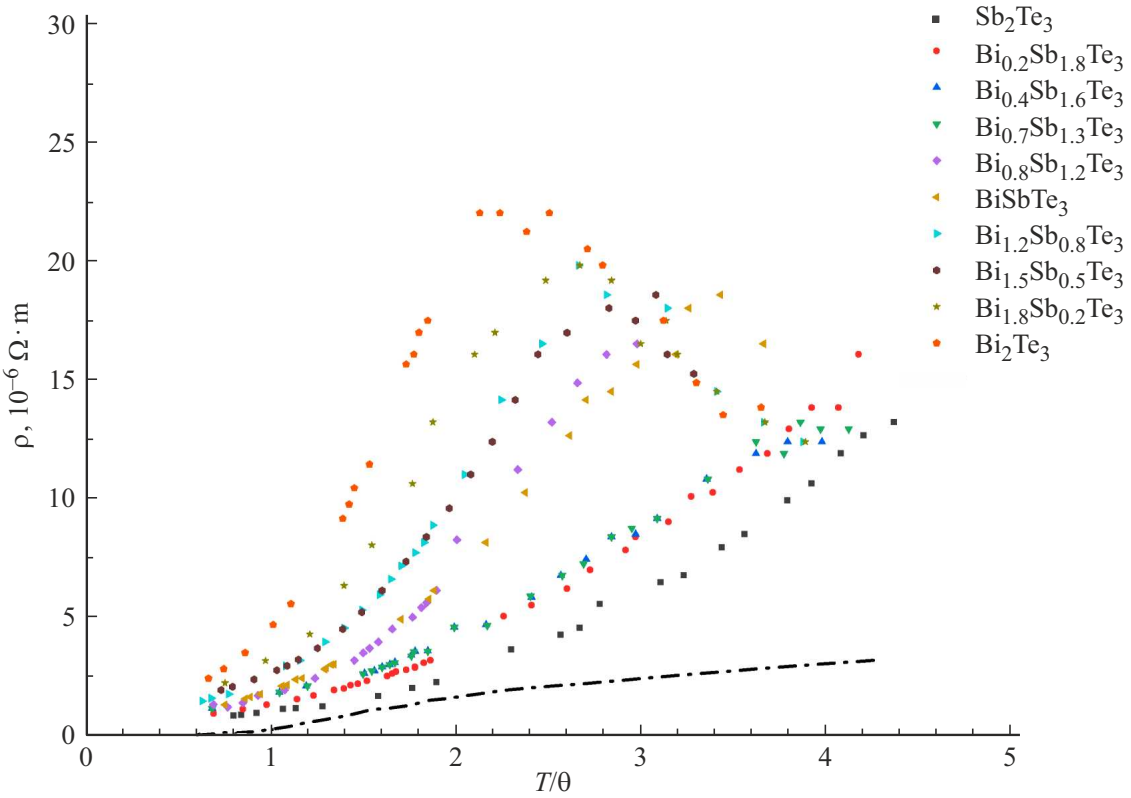

Figure 4. Dependence of resistivity of $(Bi_{2-x}Sb_x)Te_3$ $(0 < x < 2)$ solid solutions on x and the ratio between the temperature and Debye temperature θ. The variation of θ with x was taken into account [1]. The temperature dependence of resistivity of pure metals, which is characterized well by relation (3), is represented by the dash-and-dot curve.

thus also low. However, the energy of thermal vibrations at a temperature of 300 K ($kT \approx 26$ meV) is almost the same as energy gap ΔE. In line with this, the resistivity of Bi_2Te_3 crystals increases rapidly in the region of high temperatures that precede the temperatures of the onset of intrinsic conductivity (see Fig. 4). The decreasing steady-state relaxation time and concentration of light holes, which produce the dominant contribution to electric conductivity, are both conducive to this process. Specifically, the $\sum_j \left(\frac{p_j}{m_j^*}\right)$ ratio for the $Bi_{1.5}Sb_{0.5}Te_3$ crystal (see the data for it in the table) in the temperature range from 200 to 300 K varies 1.4 times faster than in the 85–150 K interval. This provides another confirmation of the above arguments regarding the influence of the transition of holes between nonequivalent extrema of the valence band on the temperature dependence of resistivity and the state of the electron system of $(Bi_{2-x}Sb_x)Te_3$ crystals.

4. Conclusion

We note in conclusion that the complex structure of the valence band of $(Bi_{2-x}Sb_x)Te_3$ crystals specifies not only the observed values of physical quantities characterizing the state of the electron system, but also the patterns of their temperature variation. The reduction in concentration of light holes at higher temperatures due to the transition of carriers between nonequivalent extrema of the valence band affects the temperature variation of the Hall coefficient, the plasma frequency, and the resistivity. Thus, the elevated electric conductivity of $(Bi_{2-x}Sb_x)Te_3$ crystals at low temperatures is attributable in part to the low intensity of the process of transition of carriers between nonequivalent extrema of the valence band. The concentration of light holes is maximized in this case. Plasmon energy $E_p = \hbar\omega_p$, which is directly proportional to light hole concentration (2), is also maximized and becomes close to the energy of carrier transition (ΔE) between the upper edge of the subband of heavy holes and the chemical potential level. As was demonstrated above, this transition affects the state of the electron system. Specifically, the plasmon energy for the $Bi_{1.5}Sb_{0.5}Te_3$ crystal at $T = 80$ K is $E_p \approx 55$ meV, and transition energy $\Delta E \approx 30$ meV. As the temperature increases, the concentration of light holes and, consequently, plasma frequency ω_p and the plasmon energy decrease (see the table), while ΔE grows (see Fig. 2). The convergence of energies of a plasmon and the interband transition in $(Bi_{2-x}Sb_x)Te_3$ crystals reflects the specifics of this thermoelectric material and intensifies the electron–plasmon interaction, thus offering valuable opportunities for its examination.

Funding

The study was supported financially by the Russian Science Foundation, grant No. 22-22-20055, https://rscf.ru/project/22-22-20055/, and the Government of Zabaykalsky Krai.

Conflict of interest

The authors declare that they have no conflict of interest.

References

[1] B.M. Gol'tsman, V.A. Kudinov, I.A. Smirnov. *Poluprovodnikovye termoelektricheskie materialy na osnove Bi_2Te_3* (M., Nauka, 1972) (in Russian).
[2] L.D. Ivanova, Yu.V. Granatkina. Inorg. Mater., **36** (7), 672 (2000).
[3] V.A. Kulbachinskii, V.G. Kytin, P.M. Tarasov, N.A. Yuzeeva. Phys. Solid State, **52** (9), 1830 (2010).
[4] G. Wang, T. Cagin. Phys. Rev. B, **76**, 075201 (2007).
[5] V.A. Greanya, W.C. Tonjes, R. Liu, C.G. Olson, D.-Y. Chung, M.G. Kanatzidis. Phys. Rev. B, **62** (24), 16425-9 (2000).
[6] P. Larson, V.A. Greanya, W.C. Tonjes, R. Liu, S.D. Mahanti, C.G. Olson. Phys. Rev. B, **65**, 085108-9 (2000).
[7] A.A. Kudryashov. Candidate's Dissertation in Mathematics and Physics: 01.04.09, Low Temperature Physics (M., Mosk. Gos. Univ., 2016) (in Russian).
[8] S.A. Nemov, N.M. Blagikh, L.D. Ivanova. Phys. Solid State, **56** (9), 1754 (2014).
[9] N.P. Stepanov, A.A. Kalashnikov, O.N. Uryupin. Semiconductors, **55** (7), 637 (2021).
[10] V.M. Grabov, A.S. Parakhin, L.S. Bagulin, O.N. Uryupin. Izv. RGPU im. A.I. Gertsena, **6** (15), 86 (2006) (in Russian).
[11] N.P. Stepanov, A.A. Kalashnikov. Opt. Spectrosc., **129**, 700 (2021).
[12] P. Lostak, J. Navratil, J. Sramkova, J. Horak. Phys. Status Solidi A, **135**, 519 (1993).
[13] P. Lostak, S. Karamazov, J. Horak. Phys. Status Solidi A, **143**, 271 (1994).
[14] L.R. Testardi, J.N. Bierly, F.J. Danahoe. J. Phys. Chem. Sol., **23**, 1209 (1962).
[15] C.H. Champness, A.L. Kipling. J. Phys. Chem. Sol., **27**, 1409 (1966).
[16] J. Ziman. *Electrons and Phonons: The Theory of Transport Phenomena in Solids* (Clarendon, 1960).
[17] F.J. Blatt. *Physics of Electronic Conduction in Solids* (McGraw-Hill, 1968).